3D Turbulence Measurements Using Three Synchronous Wind Lidars: Validation against Sonic Anemometry

FERNANDO CARBAJO FUERTES, GIACOMO VALERIO IUNGO, AND FERNANDO PORTÉ-AGEL

Wind Engineering and Renewable Energy Laboratory (WIRE), École Polytechnique Fédérale de Lausanne, Lausanne, Switzerland

(Manuscript received 25 September 2013, in final form 29 January 2014)

ABSTRACT

This paper presents a technique to measure the time series of the three components of the wind vector at a point in space from synchronous measurements of three scanning Doppler wind lidars. Knowing the position of each lidar on the ground and the orientation of each laser beam allows for reconstructing the three components of the wind velocity vector. The laser beams must intersect at the desired point in space and their directions must be noncoplanar, so that trigonometric relationships allow the reconstruction of the velocity vector in any coordinate system.

This technique has been tested during a measurement campaign carried out at Cabauw's Experimental Site for Atmospheric Research (CESAR) in the Netherlands and compared against measurements from sonic anemometers installed in a meteorological mast. The spatial resolutions of both measurement techniques differ by one order of magnitude. Therefore, in order to properly compare the results, a pseudospatial filter that mimics the attenuation induced by the lidar technology at small scales of turbulence has been applied to the velocity time series provided by the sonic anemometer.

Good agreement between both measurement systems is found in terms of the measured instantaneous velocity vector, turbulence statistics, Reynolds stresses, and the spectra of the three components of the velocity and the turbulent kinetic energy. These results provide a successful validation of the proposed technique.

1. Introduction

Researchers and industry in the fields of wind engineering and meteorology demand extensive and accurate measurements of atmospheric boundary layer turbulence for a better understanding of its role in a wide range of onshore and offshore applications: wind resource evaluation, wind turbine wakes, weather forecast, pollutant transport, urban climate studies, etc. Remote sensing techniques and especially light detection and ranging (lidar) technologies are becoming increasingly popular for the study of atmospheric flow due to their flexibility regarding transportation, installation, and operation in any type of terrain when compared to traditional meteorological masts.

Single- and dual-lidar techniques have already been successfully used to reconstruct two- or three-component wind velocity fields inside a planar or volumetric domain for a diverse range of applications, as in Newsom and Banta (2004), Newsom et al. (2005), Drechsel et al. (2010), Hill et al. (2010), and Kongara et al. (2012), and more specifically in the field of wind turbine wake measurements by Bingöl et al. (2010), Trujillo et al. (2011), and Iungo et al. (2013). Especially relevant in the field of turbulence measurement with lidars is the recent work of Mann et al. (2010), Sathe et al. (2011), Sathe and Mann (2012), and Angelou et al. (2012), in which different difficulties associated with the measurement of atmospheric turbulence with a single lidar are discussed. An extensive review of turbulence measurements with lidars can be found in Sathe and Mann (2013).

Nevertheless, up to this day, the use of three synchronous Doppler lidars with intersecting beams (hereinafter, triple-lidar technique) seems to be the only viable approach to accurately provide time series of the three components of the velocity vector at a point in space so that turbulence statistics such as turbulent kinetic energy (TKE), turbulent stresses, and velocity spectra can be calculated (Mann et al. 2009).

Corresponding author address: Fernando Porté-Agel, WIRE, EPFL, GR B2 391 (Building GR), Station 2, CH-1015 Lausanne, Switzerland.
E-mail: fernando.porte-agel@epfl.ch

DOI: 10.1175/JTECH-D-13-00206.1

2. Experimental setup

The measurements presented in this study were carried out during the month of December 2012 in Cabauw, the Netherlands.

a. CESAR observatory and meteorological mast

The Cabauw Experimental Site for Atmospheric Research (CESAR) observatory is located in the province of Utrecht (the Netherlands) in a depression 0.7 m below mean sea level. The surrounding terrain can be considered as flat and mainly covered with grass. This experimental site is equipped with a large set of instruments for the study of the atmosphere and its interaction with the land surface. Its publicly available databases provide not only turbulence measurements but also many other relevant data such as radiation, cloud height, and precipitation, which were used to assess the quality of the sonic anemometer and lidar measurements.

The central element of the research site is a 213-m-tall meteorological mast. The mast is a closed cylinder of 2-m diameter that is guyed at four levels. Equipment is mainly placed on 9.4-m-long booms that point out horizontally from the mast at three different directions (10°, 130°, and 250° from the north direction) every 20 m in height. Gill R3 sonic anemometers measuring 3D turbulence at a frequency of 10 Hz are available in the booms situated at 60, 100, and 180 m that point toward the 130° direction. The booms are long enough to reduce flow interference by the mast to about 1% at the upwind side. The boom construction itself also disturbs airflow; therefore, the actual sensor is placed at least 0.8 m above the slender boom end in order to get flow deviations that are routinely corrected, to ±1% for velocity and ±1% for wind direction (Wyngaard 1981).

More information about the site, the meteorological mast, and the instrumentation can be found in Ulden and Wieringa (1996) and Verkaik and Holtslag (2007).

b. Lidar system

Wind velocity measurements were performed using three Stream Line lidars, manufactured by Halo Photonics. These instruments are infrared pulsed Doppler wind lidars that emit wave trains with a 1.5-μm wavelength and a 15-kHz frequency. They measure the velocity component parallel to the laser beam direction, which is denoted as line of sight or radial velocity, with a resolution of 3.82 cm s^{-1}. The laser beam can be oriented toward any direction thanks to a steerable head. A pulsed wind Doppler lidar measures an average of the radial velocity along a series of equidistant gates whose length can be adjusted at will. An important characteristic of this system is its high spatial resolution; the gates can be shortened to a minimum length of 18 m. The minimum distance at which measurements are available is 45 m, and its maximum range can be extended to about 3 km depending on aerosol concentration. The sampling frequency has been set to 0.5 Hz.

c. Positioning system

Relative positions between the mast and each lidar have been determined using a Topcon's Geodetic Rover System 1 (GRS-1) GPS receiver. The declared precision is 30 cm working in a differential GPS (DGPS) network, but in practice the uncertainty in the position of each element has been noticed to be somewhat higher, probably around 1 m, and it varies depending on the number of satellites available at each time.

d. Configuration

The three lidars used are placed on the ground, equidistant to the sonic anemometer, forming an equilateral triangle. The lidar heads stare their respective beams, so that they intersect as close as possible to the sonic anemometer situated at 60 m high with an approximate 45° elevation angle. The three laser beams form a sort of regular triangular pyramid-like configuration as shown in Fig. 1.

3. Technique and data analysis

The objective of this section is to explain the processing of the measurements of the three lidars in order to calculate the three components of the wind velocity and turbulence at a point in space, and the validation of this process by comparing these results to the measurements of a sonic anemometer.

a. The meteorological coordinate system and the transformation matrix

As mentioned before, a Doppler lidar provides a measurement of the component of the velocity parallel to the laser beam V_r, which can be mathematically expressed as the projection of the actual wind velocity vector $\mathbf{V}$ in the direction of the laser beam $\mathbf{n}$:

$$V_r = \mathbf{V} \cdot \mathbf{n}. \tag{1}$$

A meteorological coordinate system is used in order to express the three components of the wind vector. These are U_m (toward east), V_m (toward north), and W_m (vertical, positive upward). The direction of the laser beam can be expressed with two angles: the elevation θ, the angle between the horizontal plane and the laser beam; and the azimuth φ, the angle between the orthogonal projection of the beam direction on the horizontal

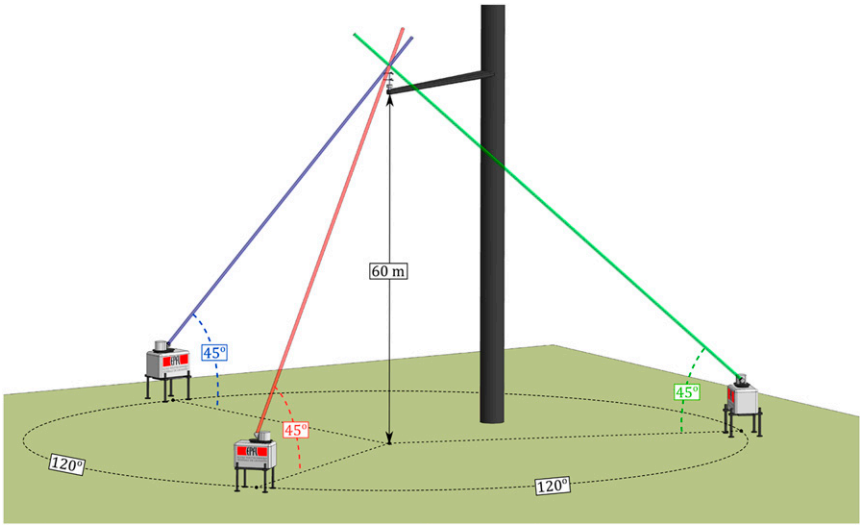

FIG. 1. The configuration of the lidars, together with the meteorological mast and the sonic anemometer.

plane and north—for example, north = 0°, east = 90°, as sketched in Fig. 2. Equation (1) for the first of the three lidars becomes

$$V_{r1} = U_m \cos(\theta_1)\sin(\varphi_1) + V_m \cos(\theta_1)\cos(\varphi_1) + W_m \sin(\theta_1). \quad (2)$$

If the wind velocity vector is known, then it can be projected onto the lidar's beam direction, but a single lidar measurement is unable to reconstruct the three unknown components U_m, V_m, and W_m. Lidar numbers 2 and 3 provide the other two equations needed to calculate them. Expressing everything in matrix form yields

$$\begin{bmatrix} V_{r1} \\ V_{r2} \\ V_{r3} \end{bmatrix} = \begin{bmatrix} \cos(\theta_1)\sin(\varphi_1) & \cos(\theta_1)\cos(\varphi_1) & \sin(\theta_1) \\ \cos(\theta_2)\sin(\varphi_2) & \cos(\theta_2)\cos(\varphi_2) & \sin(\theta_2) \\ \cos(\theta_3)\sin(\varphi_3) & \cos(\theta_3)\cos(\varphi_3) & \sin(\theta_3) \end{bmatrix} \begin{bmatrix} U_m \\ V_m \\ W_m \end{bmatrix}. \quad (3)$$

In Eq. (3) the terms on the left-hand side are the radial velocity measurements of the three lidars contained in vector $\mathbf{V}_r$ and on the right-hand side, the geometrical information in the transformation matrix $\mathbf{M}_{tr}$ and the velocity vector in meteorological coordinates $\mathbf{V}_m$. Using this notation, the previous equation can be written as

$$\mathbf{V}_r = \mathbf{M}_{tr}\mathbf{V}_m. \quad (4)$$

This equation projects the meteorological velocity vector into each lidar direction, allowing to check individually the deviations for each lidar. The inverse of the transformation matrix (denoted only as $\mathbf{M}_{tr}$, since its analytical form is cumbersome to express) allows the reconstruction of the meteorological velocity vector from the lidar measurements by

$$\mathbf{V}_m = \mathbf{M}_{tr}^{-1}\mathbf{V}_r. \quad (5)$$

Equation (5) calculates the wind velocity vector $\mathbf{V}_m$ as a simple vector–matrix multiplication, providing that the three lidars perform synchronous measurements and the laser beams are intersecting and noncoplanar; otherwise, the transformation matrix $\mathbf{M}_{tr}$ becomes noninvertible and the wind velocity vector $\mathbf{V}_m$ cannot be reconstructed.

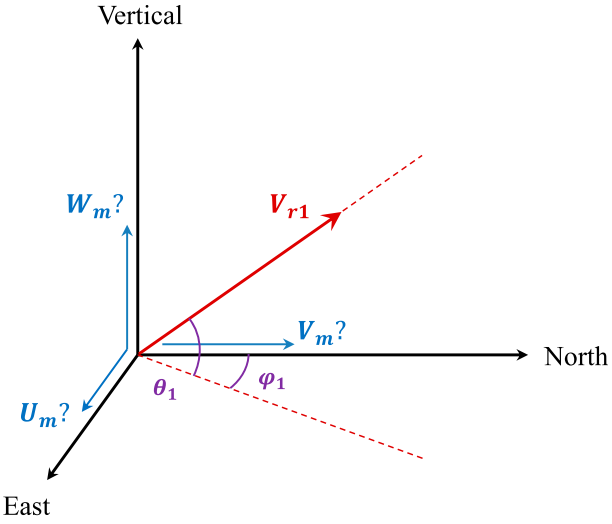

FIG. 2. The meteorological coordinate system and an arbitrary radial velocity measured by a wind Doppler lidar.

By analyzing Eqs. (3) and (5), it becomes straightforward that the error sources for the geometrical reconstruction are the measured radial velocities V_{ri} and the orientation angles of each lidar θ_i and φ_i. It should be noted that the inversion of the transformation matrix $\mathbf{M}_{\text{tr}}^{-1}$ and its multiplication by the radial velocity vector $\mathbf{V}_r$ will have the effect of propagating any of the aforementioned error sources to all three components of the velocity vector in meteorological coordinates U_m, V_m, and W_m.

b. Comparison with sonic anemometry

Spatial and temporal resolution of sonic anemometers normally ranges from 10 to 30 cm and from 10 to 100 Hz, respectively. The spatial resolution and the sampling frequency for the lidar measurements have been set to 18 m and 0.5 Hz, respectively. Therefore, it is important to correctly filter and downsample the sonic anemometer data in order to be directly comparable to the lidar measurements.

Given the spatial weighting function of the lidar system $\beta(r)$, the velocity measured by a single lidar inside an arbitrary gate at a given instant can be expressed as

$$V_{r\text{Lidar}} = \int_{-L/2}^{L/2} \mathbf{V}[(D+r)\mathbf{n}] \cdot \mathbf{n}\beta(r)\, dr, \qquad (6)$$

in which $\mathbf{V}$ is the wind velocity vector field, $\mathbf{n}$ is the unit vector in the direction of the laser beam, L is the length of the gate, D is the distance from the lidar to the gate center, and r represents a distance from the gate center along the laser beam direction. The most interesting study regarding the attenuation of the fluctuations of the radial velocity measured by a single pulsed lidar has been carried out by Mann et al. (2009), in which they make use of a well-known atmospheric turbulence model by Mann (1994).

Nevertheless, the reconstruction of the three components of the velocity vector is obtained from a combination of three one-dimensional convolutions [Eq. (6)] corresponding to the three lidars, with which it is difficult to deal. Therefore, a single three-dimensional convolution window $\psi(r)$ has been used to substitute the effect of combining three one-dimensional convolutions and the uncertainty in the position of the lidars, δ. In practice $\psi(r)$ treats the three lidars as a single system and therefore assumes a single spherical measuring volume of diameter $L + 2\delta$ represented by a truncated Gaussian convolution window:

$$\psi(r) = e^{-(1/2)\{A[r/(L+2\delta)]\}^2}, \qquad (7)$$

where A determines the shape of the window and r is the distance from the center of the window, that is, the point where the laser beams intersect. The A factor is equal to 5. It has been estimated as a fit to an average of the three individual weighting functions associated to the range gates of the three lidars. Those functions are shifted in space a distance δ, equal to the positioning accuracy of the experimental setup. For our experiments δ was equal to 1 m. This value may be adapted for different lidar systems. The spatial filtering induced by the triple-lidar technique can be therefore expressed as

$$\mathbf{V}_{\text{Lidar}} = \int_{-(L+2\delta)/2}^{(L+2\delta)/2} \int_0^{2\pi} \int_0^{\pi/2} \mathbf{V}(\mathbf{R}+\mathbf{r}) \frac{\psi(r)}{C} dr\, d\varphi\, d\theta, \qquad (8)$$

where C is the value needed to normalize the convolution window ψ each time, $\mathbf{R}$ indicates the position of the center of the Gaussian convolution window, and $\mathbf{r}$ is a vector with its origin in the center of the same window expressed in spherical coordinates r, φ, and θ. This has the advantage of not needing to make use of a turbulence model, being this one of the concerns expressed in Sathe and Mann (2013).

Currently, there is not such a measurement technique that allows an instantaneous measurement of the wind velocity vector field $\mathbf{V}$ in three dimensions inside a sphere of ~20-m diameter with an acceptable resolution—at least one order of magnitude smaller than the lidar resolution—that would allow the calculation of the three-dimensional convolution proposed in Eq. (8). Therefore, two more assumptions are used: flow homogeneity inside the spherical domain where the laser beams cross and Taylor's hypothesis. This allows the three-dimensional Gaussian convolution window in space to become a single Gaussian convolution window in time. Then, the measurements from a single sonic anemometer can be convolved to be directly comparable to the triple-lidar technique by

$$\mathbf{V}_{\text{Lidar}}(t) \simeq \mathbf{V}_{\text{Sonic,filt}}(t) = \int_{-(L+2\delta)/(2\overline{U}_h)}^{(L+2\delta)/(2\overline{U}_h)} \mathbf{V}_{\text{Sonic}}(t+\tau) \frac{\psi(t)}{C} d\tau, \qquad (9)$$

where $t = r/\overline{U}_h$. Equation (9) is in fact a pseudospatial filtering (time filtering in practice) of the sonic data. This process is sketched in Fig. 3.

4. Results

The triple-lidar technique described above has been used to measure remotely the wind velocity close to

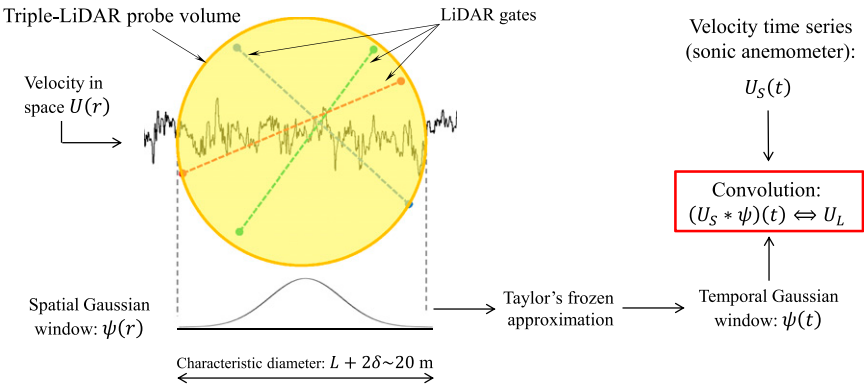

FIG. 3. The pseudospatial filtering applied to one of the velocity components measured by the sonic anemometer.

a sonic anemometer installed in Cabauw's meteorological mast at a 60-m height on 14 December 2012 from 0000 to 0100 UTC + 1. The wind direction during the test oscillated between 120° and 150°, guaranteeing no flow perturbation of the incoming wind by the mast (see section 2). The three components of the velocity vector have been calculated in meteorological coordinates U_m, V_m, and W_m first. Then, the horizontal components have been transformed to streamline coordinates longitudinal U_{str} and transversal V_{str} by a simple rotation using the average wind direction measured by the sonic anemometer.

a. *Instantaneous velocity vector*

Figure 4 presents a comparison of the three components of the wind velocity vector in time measured by the sonic anemometer and the triple-lidar technique. The unfiltered sonic signal shows higher variance due to its higher spatial and temporal resolution. Those measurements have been filtered as explained in the previous section and downsampled to match the sampling frequency (0.5 Hz) of the lidars. There is a good agreement between both techniques.

b. *Turbulence statistics*

The differences between the statistics calculated from the sonic and the lidar measurements are presented in Table 1. The differences between the sonic and lidar averages in terms of wind velocity or direction are very small, below the velocity resolution (3.8 cm s^{-1}) of the lidar system. This is possible if there is no bias in the measurements and the velocity fluctuations are bigger than the lidar resolution itself.

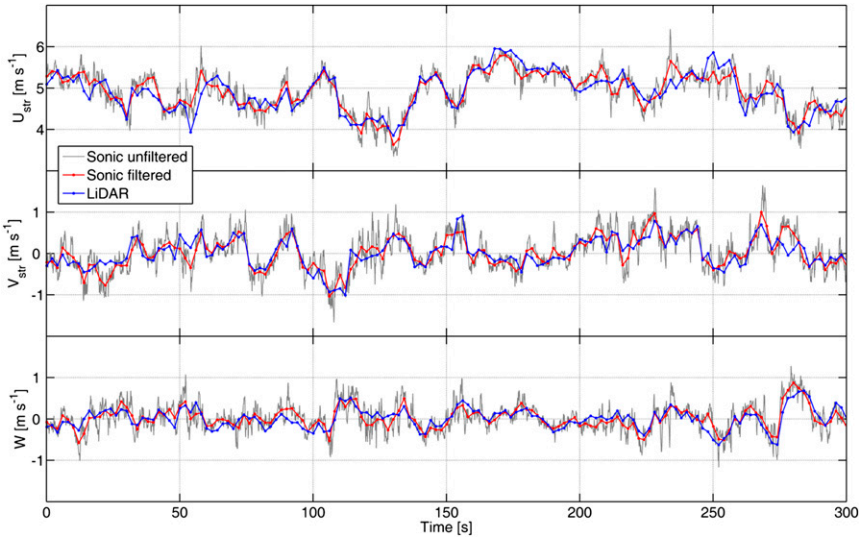

FIG. 4. Example of the reconstructed components of the velocity vector in streamwise coordinates with the triple-lidar technique against filtered and unfiltered measurements by the sonic anemometer (only 5 min presented).

TABLE 1. Differences in statistics of wind speed and direction between the sonic anemometer measurements and the lidar technique proposed. Note that the differences calculated are always between the filtered sonic data and the lidar measurements.

	Averages		
	Sonic filtered and unfiltered	Lidar	Difference
$\overline{U}_{str}$ (m s^{-1})	5.03	5.06	0.03
$\overline{V}_{str}$ (m s^{-1})	0.00	0.01	0.01
$\overline{W}$ (m s^{-1})	0.02	0.02	0.00
Wind direction (°)	135.34	134.32	−1.02
	Standard differences (instantaneous values)		
	Sonic filtered–lidar		
U_{str} (m s^{-1})	0.17		
V_{str} (m s^{-1})	0.13		
W (m s^{-1})	0.09		
Wind direction (°)	1.64		
	Turbulence intensities		
	Sonic unfiltered	Sonic filtered	Lidar	Difference
$I_{U_{str}}$(%)	10.3	9.6	9.9	0.3
$I_{V_{str}}$(%)	8.3	6.9	5.9	−1.0
I_W (%)	6.3	4.8	4.7	−0.1
	Other turbulence quantities			
	Sonic unfiltered	Sonic filtered	Lidar	Difference
$\overline{u'v'}$ (m^2 s^{-2})	−0.0217	−0.0219	−0.0241	−0.0023
$\overline{v'w'}$ (m^2 s^{-2})	0.0351	0.0243	0.0177	−0.0066
$\overline{u'w'}$ (m^2 s^{-2})	−0.0431	−0.0396	−0.0515	−0.0119
TKE (m^2 s^{-2})	0.274	0.206	0.198	−0.008

The standard differences for the instantaneous velocity components and direction between the filtered sonic measurements and the lidar ones also show a good agreement. The standard errors are on the order of $0.1 \sim 0.2$ m s^{-1} for the velocities and less than 2° for the direction.

The turbulence intensities show that, as expected, the filter applied to the sonic measurements and the inherent spatial filter of the lidar technique attenuates the turbulence fluctuations for all three components of the velocity. There is good agreement between the turbulence intensities calculated using the filtered sonic measurements and the lidars, with a maximum of 1% underestimation in the transversal component V_{str} by the lidars. The rest of the turbulence quantities calculated agree well too, finding the biggest difference on the $\overline{u'w'}$ turbulent flux and the smallest on the TKE.

c. *Turbulence spectra*

Figure 5 shows the turbulence spectra for each velocity component as well as for the turbulent kinetic energy. It is possible to observe the anisotropy of the big scales of the flow and also the characteristic $-2/3$ slope of the inertial subrange at smaller scales. The unfiltered sonic anemometer measurements resolve several decades of the inertial subrange, whereas in this case the lidar spatial and temporal resolution covers only around one decade. This range might be slightly wider or narrower depending on several factors like, for instance, the mean advection velocity, the Reynolds number, the measurement height, or the atmospheric stability.

The filtered sonic and lidar spectra agree very well for the whole range of frequencies and decay in the same manner for frequencies higher than 0.1 Hz. This indicates that the pseudospatial filtering performed on the sonic measurements mimics well the real behavior of the spatial filtering induced by the lidar technique for turbulence scales in the order of 20 m and less.

5. Conclusions

The present work describes a technique for the measurement of the three components of the instantaneous wind velocity vector at a point in space. It is based on a trigonometrical reconstruction procedure applied to simultaneous measurements of three Doppler lidars whose beams are intersecting.

The results of the technique have been compared to sonic anemometer measurements at a height of 60 m

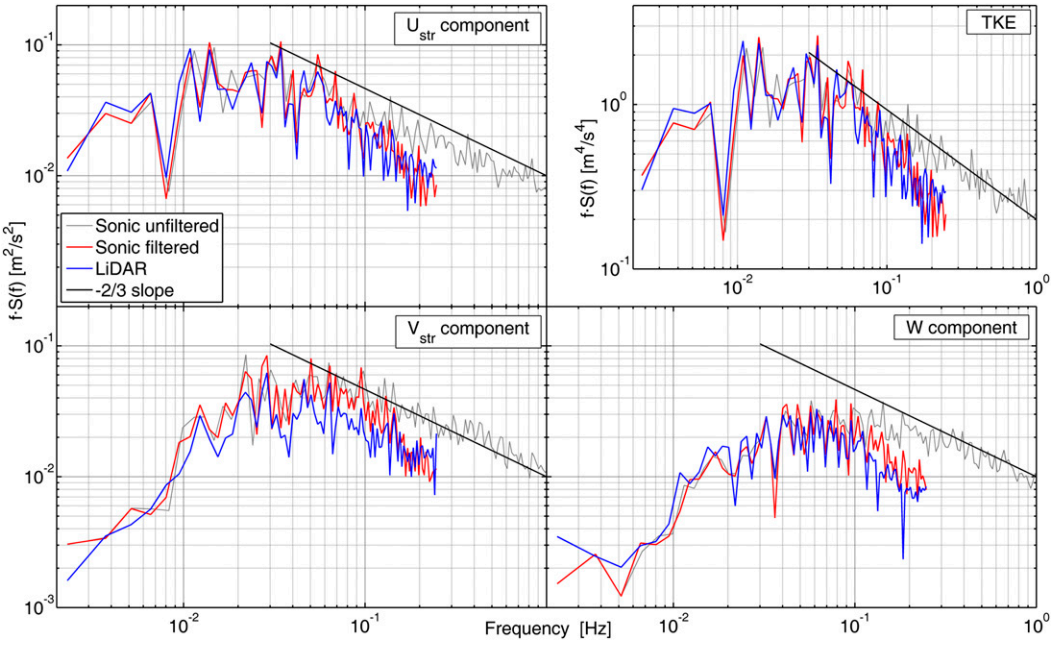

FIG. 5. Spectra of the longitudinal, transversal, and vertical components of the wind velocity as well as turbulent kinetic energy measured with the triple-lidar technique against filtered and unfiltered measurements by the sonic anemometer together with the characteristic $-2/3$ slope of the inertial subrange.

over flat terrain. Because of the different spatial and temporal resolutions of both measurement techniques, the sonic anemometer measurements have to be filtered and downsampled in order to be comparable to the lidar measurements for validation purposes. This is done via a convolution of the time series of the velocity measured by the sonic anemometer and a Gaussian spatial convolution window that represents the lidar attenuation of the turbulence at small scales. To apply properly this convolution, the spatial window is converted to a time window using Taylor's hypothesis and assuming flow homogeneity inside the measurement volume. The good agreement between both triple-lidar and sonic anemometer measurements in terms of averages, instantaneous values, and different turbulent quantities, as well as turbulence spectra provides a validation of the proposed technique.

Future work will address the error propagation in the reconstruction procedure of the velocity vector and a detailed uncertainty analysis of the technique. The different error sources of the technique will be considered as well as the influence of different configurations of the setup and filtering of the sonic measurements.

Acknowledgments. The authors kindly acknowledge the Royal Netherlands Meteorological Institute (KNMI) and especially Fred Bosveld and Alfons Driever for all the practical help provided during the measurement campaign as well as for the discussions regarding sonic anemometry issues at CESAR's meteorological site.

This research was supported by the Swiss Federal Office of Energy under the Project REF-1081-00221.

REFERENCES

Angelou, N., J. Mann, M. Sjöholm, and M. Courtney, 2012: Direct measurement of the spectral transfer function of a laser based anemometer. *Rev. Sci. Instrum.,* **83,** 033111, doi:10.1063/1.3697728.

Bingöl, F., J. Mann, and G. Larsen, 2010: Light detection and ranging measurements of wake dynamics part I: One-dimensional scanning. *Wind Energy,* **13,** 51–61, doi:10.1002/we.352.

Drechsel, S., G. J. Mayr, M. Chong, and F. K. Chow, 2010: Volume scanning strategies for 3D wind retrieval from dual-Doppler lidar measurements. *J. Atmos. Oceanic Technol.,* **27,** 1881–1892, doi:10.1175/2010JTECHA1495.1.

Hill, M., R. Calhoun, H. J. S. Fernando, A. Wieser, A. Dörnbrack, M. Weissmann, G. Mayr, and R. Newsom, 2010: Coplanar Doppler lidar retrieval of rotors from T-REX. *J. Atmos. Sci.,* **67,** 713–729, doi:10.1175/2009JAS3016.1.

Iungo, G. V., Y.-T. Wu, and F. Porté-Agel, 2013: Field measurements of wind turbine wakes with lidars. *J. Atmos. Oceanic Technol.,* **30,** 274–287, doi:10.1175/JTECH-D-12-00051.1.

Kongara, S., R. Calhoun, A. Choukulkar, and M. Boldi, 2012: Velocity retrieval for coherent Doppler lidar. *Int. J. Remote Sens.,* **33,** 3596–3613, doi:10.1080/01431161.2011.631948.

Mann, J., 1994: The spatial structure of neutral atmospheric surface-layer turbulence. *J. Fluid Mech.,* **273,** 141–168, doi:10.1017/S0022112094001886.

——, and Coauthors, 2009: Comparison of 3D turbulence measurements using three staring wind lidars and a sonic anemometer. *Meteor. Z.,* **18,** 135–140, doi:10.1127/0941-2948/2009/0370.

——, A. Peña, F. Bingöl, R. Wagner, and M. S. Courtney, 2010: Lidar scanning of momentum flux in and above the atmospheric surface layer. *J. Atmos. Oceanic Technol.,* **27,** 959–976, doi:10.1175/2010JTECHA1389.1.

Newsom, R., and R. Banta, 2004: Assimilating coherent Doppler lidar measurements into a model of the atmospheric boundary layer. Part I: Algorithm development and sensitivity to measurement error. *J. Atmos. Oceanic Technol.,* **21,** 1328–1345, doi:10.1175/1520-0426(2004)021<1328:ACDLMI>2.0.CO;2.

——, D. Ligon, R. Calhoun, R. Heap, E. Gregan, and M. Princevac, 2005: Retrieval of microscale wind and temperature fields from single-and dual-Doppler lidar data. *J. Appl. Meteor.,* **44,** 1324–1345, doi:10.1175/JAM2280.1.

Sathe, A., and J. Mann, 2012: Measurement of turbulence spectra using scanning pulsed wind lidars. *J. Geophys. Res.,* **117,** D01201, doi:10.1029/2011JD016786.

——, and ——, 2013: A review of turbulence measurements using ground-based wind lidars. *Atmos. Meas. Tech.,* **6,** 3147–3167, doi:10.5194/amt-6-3147-2013.

——, ——, J. Gottschall, and M. S. Courtney, 2011: Can wind lidars measure turbulence? *J. Atmos. Oceanic Technol.,* **28,** 853–868, doi:10.1175/JTECH-D-10-05004.1.

Trujillo, J., F. Bingöl, G. Larsen, J. Mann, and M. Kühn, 2011: Light detection and ranging measurements of wake dynamics. Part II: Two-dimensional scanning. *Wind Energy,* **14,** 61–75, doi:10.1002/we.402.

Ulden, A., and J. Wieringa, 1996: Atmospheric boundary layer research at Cabauw. *Bound.-Layer Meteor.,* **78,** 39–69, doi:10.1007/BF00122486.

Verkaik, J. W., and A. A. M. Holtslag, 2007: Wind profiles, momentum fluxes and roughness lengths at Cabauw revisited. *Bound.-Layer Meteor.,* **122,** 701–719, doi:10.1007/s10546-006-9121-1.

Wyngaard, J., 1981: The effects of probe-induced flow distortion on atmospheric turbulence measurements. *J. Appl. Meteor.,* **20,** 784–794, doi:10.1175/1520-0450(1981)020<0784:TEOPIF>2.0.CO;2.